Available online at www.sciencedirect.com

SciVerse ScienceDirect

Procedia Engineering 55 (2013) 443 – 450

Procedia Engineering

www.elsevier.com/locate/procedia

6th International Conference on Creep, Fatigue and Creep-Fatigue Interaction [CF-6]

Burst and Biaxial Creep of Thin-Walled Tubing of Low c/a-Ratio HCP Metals

K. Linga Murty[a*], C.S. Seok[b] and B. Kombaiah[a]

[a]*North Carolina State University, Raleigh NC 27695-7909, USA*
[b]*Sungkyunkwan University, Suwon, Republic of Korea*

Abstract

Thin-walled tubing used in various structures are made of low c/a-ratio hcp metals such as Zr and Ti based alloys, and their integrity to internal pressures is of prime importance in the life of these engineering structures. We summarize here some of the work performed on Zircaloy cladding commonly used in LWRs as thin walled tubing as well as Cp-Ti and Ti3Al2.5V that find applications in aerospace industry. Considered here are three different types of tests: (i) burst tests using closed-end internal pressurization, (ii) uniaxial ring tests for characterization of hoop creep properties and (iii) hoop creep under biaxial internal pressurization. Burst and ring tests yielded identical hoop creep and rupture characteristics indicating the utility of ring tests to replace burst tests. Importance of transitions in creep mechanisms with decreased stress levels in predicting in-service dimensional changes is emphasized.

Keywords: Zircaloys; titanium; burst; biaxial creep; microstructure

1. Introduction

Several thin walled tube structures in nuclear and aerospace applications are made of Zirconium and Titanium alloys respectively due to their attractive properties. Zircaloys (Zircaloy-2 and Zircaloy-4) are primarily used as fuel cladding tubes and core internals in light water reactors (LWR) while Nb additions have been noted to improve long term corrosion resistance and better mechanical properties [1, 2]. Similarly, Titanium and its alloys are used as gas carrying tubes in aerospace and chemical industries due to their high strength to weight ratio and good corrosion resistance [3]. In many of these applications, creep deformation of the tube structures becomes critical due to the combined application of mechanical stress and temperature. In addition, these structures are subject to complex multiaxial stresses due to external and internal pressures along with axial forces due to end caps etc [4]. Since many of these tube structures are thin-walled (meaning diameter larger by more than 10 times thickness), radial or thickness stresses are negligible leading to biaxial (hoop and

* *Corresponding Author:*
E-mail address: murty@ncsu.edu

doi:10.1016/j.proeng.2013.03.278

axial) stresses. Thus, understanding the creep behavior in particular under closed end internal pressurization is indispensible for designing long safe running reactors and other structures.

In this article, the burst and creep characteristics of thin-walled tubing of Zr and Ti based alloys are presented with emphasis on transitions in creep mechanisms as lower stresses corresponding to in-service conditions are approached. Also considered here are the hoop burst and creep characteristics using both internal pressurization of tubing as well as uniaxial hoop (ring) creep and rupture tests. Burst and creep rupture data are analyzed in terms of Larson-Miller parameter while transitions in creep mechanisms in internally pressurized Ti3Al2.5V tubing revealed the significance of deformation microstructures in unequivocally characterizing the underlying micromechanism(s) of creep [5]. It has been recognized that the burst properties of tubes are strongly related to the creep properties along the hoop direction [6] while ring creep tests are useful in evaluating creep properties along the hoop direction [7].

2. Materials and experiments

Biaxial burst and creep tests were performed on the Zirconium and Titanium alloys listed in Table 1 along with their compositions. Biaxial creep tests are conducted by internally pressurizing closed end tubes with in-situ measurement of hoop and axial strains using Laser telemetric and LVDT extensometers [1,5] (Fig. 1a). Internal pressurization of tubing gives rise to a stress ratio (i.e. hoop stress to axial stress) of 2:1 and since in all cases the axial strains are negligibly small, further discussions are confined to hoop strains only [5]. Burst test is similar to the biaxial test and it is useful in predicting the short term creep rupture characteristics [8]; however, here the test is continued till fracture of the tube with only post-test measurement of hoop strains. Ring creep tests were performed to evaluate the properties in the hoop direction at various temperatures (350-600 ^{o}C) [9]. The test involves application of tensile force in the hoop direction of specially machined ring specimens (Fig. 1b). The details of the test configuration and method have been described elsewhere [7] and appropriate calibration was made to take care of bending displacements of the device and the ring [10].

Table 1. Details of the materials tested in this study and the testing conditions.

Tubing	Processed Condition	Chemical composition (wt%)	Tests	Test temperature (K)
Zircaloy-4	Recrystallized at 973 K for 4 hrs	Zr-1.5Sn-0.21Fe-0.1Cr-0.01O	Burst	523-773K
Zirlo	Cold worked stress relieved	Zr-1Sn-1Nb-0.01Fe-0.008C -0.01O	Burst and Ring creep	523-873K
Cp-Ti	Recrystallized	Ti-0.2Fe-0.18O-0.1C-0.01H-0.03N	Burst	523-773K
Ti3Al2.5V	Recrystallized at 973 K for 4 hrs	Ti-2.91Al-2.42V-0.12O-0.05C-0.03Fe-0.02N-0.013H	Biaxial creep	723-873K

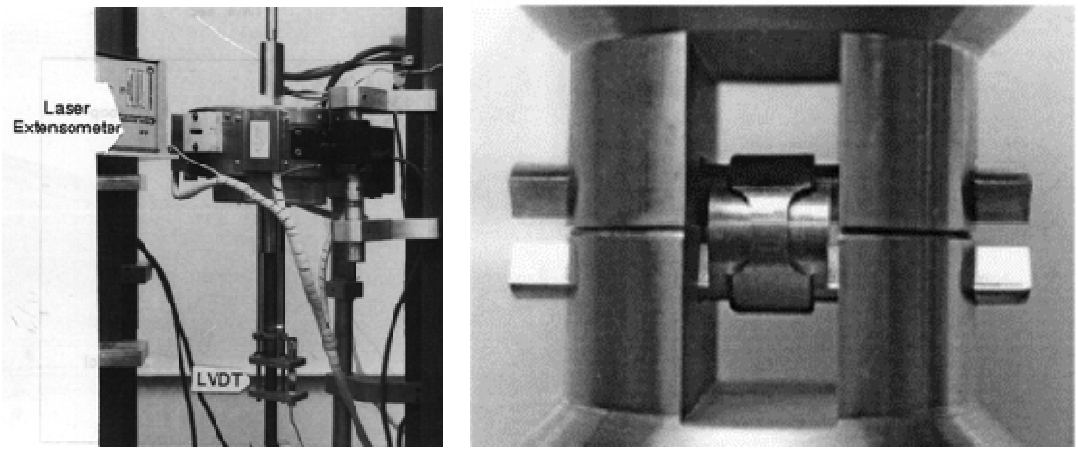

Fig. 1. (a). Biaxial Creep System and (b) Ring Creep Test Assembly.

2.1. Burst and ring creep tests

Burst tests were carried out on Zircaloy-4, Zirlo and Cp-Ti to investigate the creep rupture behavior of these materials using closed end tubes of ~9.5 mm of outer diameter and ~0.6 mm of wall thickness by internally pressurizing using Argon gas for various pressures at a range of temperatures (~300°C-600°C). Each test was carried out till the tube fractures to estimate the creep rupture time. The test duration was recorded using a timer. The details of the burst set up are described elsewhere [6]. The diameter of the tube specimen was measured across its length before and after the burst test for calculating the uniform circumferential elongation (UCE) from which the steady state strain rate ($\dot{\varepsilon}$) was calculated by dividing the UCE by the rupture time, t_r,

$$\dot{\varepsilon} = \frac{UCE}{t_r} = \frac{\ln\left(\frac{d}{d_0}\right)}{t_r}, \quad (1)$$

where d is the average uniform diameter of the burst specimen and d_0 is the original diameter of the un-burst specimen. The burst hoop stress (σ_θ) applied on the tubes was calculated using thin-wall approximation,

$$\sigma_\theta = \frac{pd}{2t}, \quad (2)$$

where p is the internal pressure, d is the mean diameter and t is the tube thickness. The creep data along the hoop direction in tubes can be obtained using the ring creep test setup which involves applying tensile stress in the hoop direction of the ring specimens machined from tubes (Fig. 1b). The biaxial burst and uniaxial ring creep tests were performed on Zirlo alloy at identical temperature and hoop stress conditions in order to compare these two data sets [9]. The creep rupture data obtained from both the burst and ring tests were fit to Larson-Miller parameter (Eq. 3) which is a useful design parameter to predict the creep rupture time at different stresses and temperatures,

$$LMP = T(\log t_r + C). \quad (3)$$

Here T is test temperature (K), t_r is the rupture time in hours and C is a constant (~20).

2.2. Biaxial creep test

Biaxial creep tests on recrystallized Ti3Al2.5V tubes were carried out in a temperature range 723–873 K by closed end gas pressurization with Argon. The grain size of the recrystallized Ti3Al2.5V was measured to be 6.6±0.4 μm using the linear intercept method. Hoop strains were monitored in-situ using a Lasermike and the tube specimens tested at 873 K were coated with gold in a pulsed laser deposition chamber to avoid oxidation issues [5]. Deformation microstructures were studied using TEM of samples prepared using mechanical and electro jet polishing procedures from the gage section of the tube. TEM imaging was carried out in order to correlate and explain the active creep deformation mechanisms [5].

3. Results and discussion

3.1. Burst and ring creep

Figure 2a comprises the rupture data plotted as LMP versus hoop stress for Zirlo and Zircaloy-4 both in cold-worked stress-relieved (CWSR) and recrystallized (Rx) conditions obtained from burst and ring creep

tests [9]. We note three important features: (i) Rx material exhibits a change in slope as lower stresses are approached, (ii) overlapping of LMP of Zirlo and Zircaloy-4 suggests that Nb additions to Zircaloys have negligible effect on their creep life, and (iii) both burst and ring creep tests agreed extremely well revealing the significance of ring tensile and creep tests to yield information on hoop behavior under biaxial loading that is commonly encountered in-reactor. The 3rd observation here is of importance in characterizing hoop deformation of highly irradiated materials since ring tests require relatively small amount of material compared to burst tests. Similar LMP plot for Cp-Ti is shown in Fig. 2b [6].

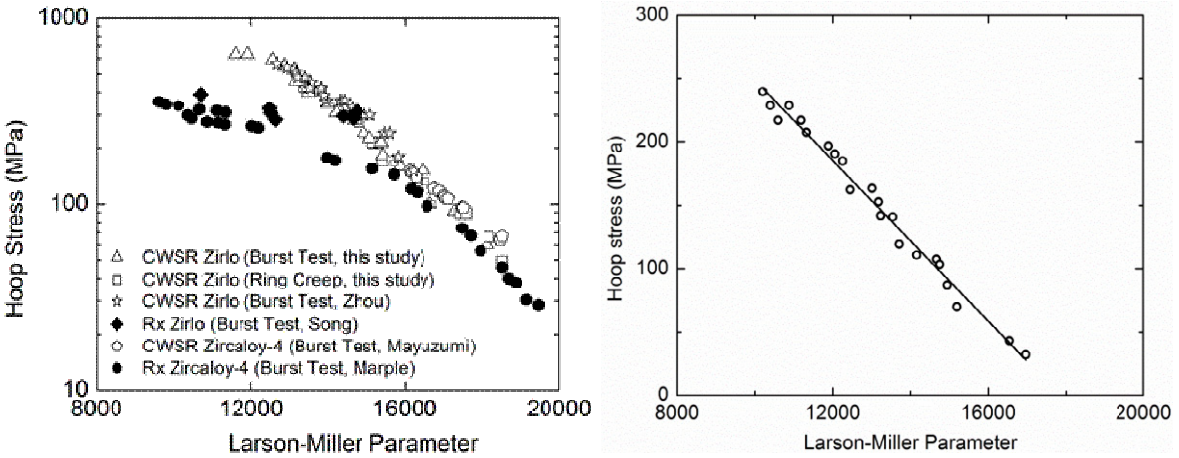

Fig. 2. Hoop Stress vs Larson-Miller Parameter for (a) Zirlo and Zircaloy-4 and (b) Cp-Ti.

The minimum or steady state creep rates obtained from the ring and burst tests were analyzed in terms of dimensionless Dorn parameters:

$$\frac{\dot{\varepsilon}kT}{DEb} = A\left(\frac{\sigma}{E}\right)^n, \qquad (4a)$$

where D is the appropriate diffusivity, E the temperature dependent elastic modulus, b the Burgers vector, k Boltzmann's constant, T the temperature in K and A is the dimensionless constant dependent on the underlying creep mechanism. Figure 3a includes the creep data of Zirlo plotted as normalized creep-rate versus normalized hoop stress and demonstrates the equivalence between uniaxial ring creep and biaxial burst test results. We note the power law creep with n=6 at low stresses with the power-law breakdown at higher stresses ($>10^{-2}$E). A similar plot for Cp-Ti is included in Fig. 3b depicting again the power law breakdown at higher stresses.

The power law regime with stress exponent 6 for Zirlo and 7 for Cp-Ti suggests that the dislocation climb controlled creep mechanism [14] is operative with the characteristic power-law breakdown at higher stresses. The activation energy for creep of Zirlo was estimated to be 58 Kcal/mol which is close to the activation energy for self diffusion [8]. Formation of distinct subgrains in the power-law creep regime confirmed the operation of dislocation climb mechanism as depicted in Fig. 4 of the dislocation substructure in Cp-Ti using transmission electron microscopy (TEM) following creep at 70.6 MPa and 773 K (equivalent to σ/E of 9×10^{-4}). It is to be noted that such subgrain formation is not observed in class-I alloys when viscous glide controlled creep (microcreep with n~3) dominates [19].

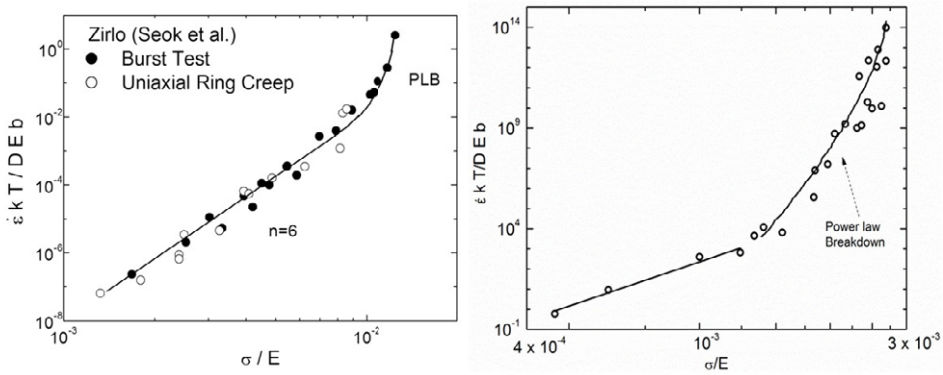

Fig. 3. Hoop Creep Results Plotted in Terms of Dorn parameters for (a) Zirlo (burst and ring tests) and (b) Cp-Ti (burst).

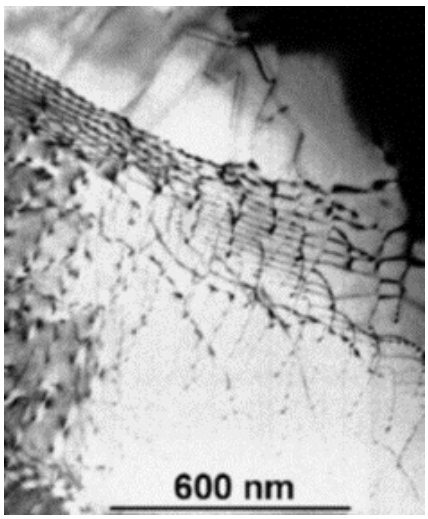

Fig. 4. A bright field TEM image of Cp-Ti showing sub-grain formation at 70.6 MPa and 773K in the power law regime.

3.2. Ti3Al2.5V Hoop creep results

Hoop creep data on recrystallized Ti3Al2.5V tubing under (2:1)-loading were obtained at varied temperatures and stresses to cover 2 orders of magnitude of stress from around 10^{-4}E to 10^{-2}E, and gold plating on the gauge sections prevented problems with oxidation. The results were analyzed in terms of Dorn parameters and a double-log plot of dimensionless strain-rate versus stress revealed 3 distinct regimes with stress exponents of 1, 2 and 5 [5]. Figure 5 includes these results along with deformation microstructures observed at different stress levels in various regimes.

It is to be noted that the activation energy was measured to be 232±25 kJ/mole at low stresses in regions I and II while it was seen to be 325±20 kJ/mole in the high stress region III [5]. The higher value was identified to be that for self-diffusion in Ti while the lower value corresponds to that for grain boundary diffusion; it is well known that the activation energy for grain-boundary diffusion is around 50-70% of that for lattice self-diffusion [15]. From the measured values of the stress exponent and activation energy, it is possible to predict the active deformation mechanism(s) in the different regions. At intermediate stresses in region II with a stress exponent of 2 and an activation energy of 232±25 kJ/mole, it is suggested that the deformation is controlled by grain boundary sliding (GBS) which is also in conformation with the deformation microstructure that revealed extensive dislocation activity near grain-boundaries (Fig. 5).

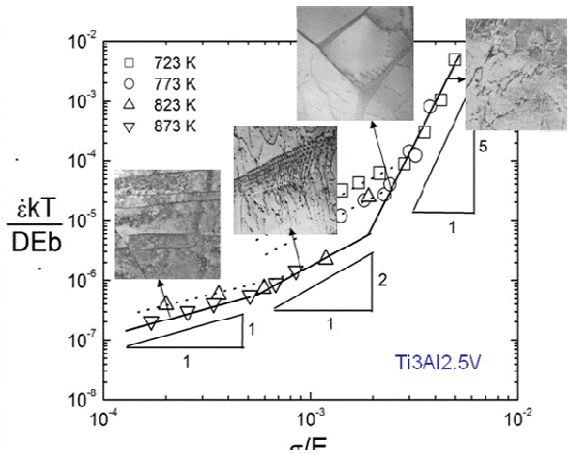

Fig. 5. Normalized strain-rate versus stress depicting transitions in creep mechanisms in Ti-3Al-2.5V along with deformation microstructures at various stress levels

The creep rates in region II reveal a good correlation with GBS model by Ruano and Sherby [11],

$$\dot{\varepsilon}_{GBS} = 10^8 \frac{D_{GB} b}{(GS)^2} \left(\frac{\sigma}{E} \right)^2, \tag{4b}$$

where GS is the grain-size, D_{GB} is the grain-boundary diffusivity.

With identical activation energy for grain boundary slidin g and a stress exponent of 1 in region I, it was first thought Coble creep should be the rate controlling process; however, the creep rates predicted by Coble creep were 3 orders of magnitude lower than the experimental results [12]. Moreover, deformation microstructures revealed dislocation activity in terms of slip band formation (Fig. 5) with the slip band spacing measured to be 250±50 nm from the TEM micrographs. HRTEM study confirmed that they are indeed slip bands and not twins. These creep data in region I were thus fit to the Spingarn-Nix slip-band model [13] based on the climb of dislocations at intersections of the slip bands and grain boundaries (Fig.6),

$$\dot{\varepsilon}_{SB} = 50 \frac{(GS) D_{GB} \Omega \delta}{\lambda^4 kT} \sigma. \tag{5}$$

Here λ is the slip band spacing (250 nm), Ω is the atomic volume, δ is the grain boundary width and all other terms have already been defined and we note an excellent correlation between the experimental results and slip-band model predictions.

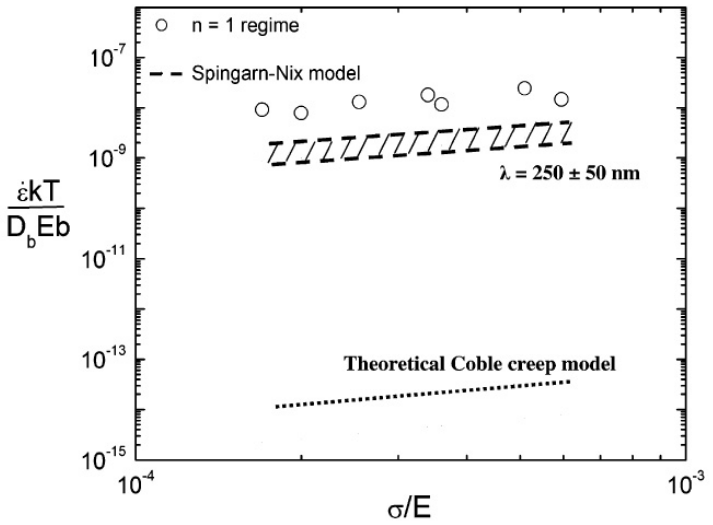

Fig. 6. Correlation of region I experimental creep data with predictions of Coble creep model and Spingarn-Nix model with slip band spacing (λ_{SB}) of 250 nm.

At high stresses in region III the creep-rates followed the power-law equation with n~5 and $Q=Q_D$,

$$\dot{\varepsilon}_{III} = 1.7x10^{9}\frac{DEb}{kT}\left(\frac{\sigma}{E}\right)^{5}. \tag{6}$$

With n around 5 and the activation energy for creep identified to be that for lattice diffusion, the rate controlling mechanism is identified to be the climb of edge dislocations [14]. TEM studies in this region however revealed two distinct types of dislocation microstructures depending on the stress level. In the low stress end of region III at $\sigma=3.02x10^{-3}E$, subgrains of size 1.2 μm were noted that followed the standard empirical relation valid when Weertman edge dislocation climb creep mechanism controls creep [15],

$$\frac{\delta_{SG}}{b} = 20\left(\frac{\sigma}{E}\right)^{-1}, \tag{7}$$

where δ_{SG} is the subgrain size. On the other hand, at high stresses in region III with n=5 and $Q_c=Q_D$, dispersed dislocations mainly long screw type were noted (Fig. 5) indicative of jogged screw dislocation model where the climb of jogs on screw dislocations controls the creep rate [16,17]. The jogged screw dislocation creep model originally put forth by Barrett and Nix has been modified by Karthikeyan et al [18] according to which the creep-rates are given by,

$$\dot{\varepsilon}_s = \frac{\pi D}{\beta b h_d}\left(\frac{\sigma}{\alpha G}\right)^{2}\left[\exp\left(\frac{\sigma\Omega\lambda_{jog}}{4\beta h_d kT}\right)-1\right]. \tag{8}$$

Here D is lattice diffusivity, h_d is the maximum jog height that can be achieved for a given stress level, α and β are constants, G is the shear modulus, Ω is the atomic volume, λ_{jog} is the jog spacing and the rest of the terms are the same as defined previously. The average jog height is represented as βh_d. Although the jogged screw

dislocations observed here at high stresses are not well formed, we believe that the absence of subgrain boundaries reveals the change in the creep mechanism in region III at high stress end compared to that at the lower stress range. These observations clearly point out that in some cases there may be a possible transition in creep mechanism that is too subtle to be revealed as a marked change in the stress exponent and can only be revealed by careful studies of dislocation microstructures following creep deformation.

It is seen from the analysis of creep data and microstructural investigations on Ti3Al2.5V that there are transitions in creep mechanisms depending on the applied stress and temperature from a dislocation glide-climb creep at higher stresses to a GBS-controlled mechanism at intermediate stresses to a diffusion controlled viscous creep at lower stresses. Such transitions in the rate controlling creep mechanisms were also found in Zirlo [8, 19], Zircaloy-4 [20] and Cp-Ti [6] using burst and ring tests. It is important to recognize that blind extrapolation of high stress data to low stresses corresponding to those encountered in service could result in non-conservative predictions of creep-rate and creep life, and thus the transitions in creep mechanisms must be considered while extrapolating the creep data to predict the rupture time of the structures in-service. Just a linear extrapolation of creep data would be invalid and is potentially dangerous while designing the critical structures in nuclear reactors and aircrafts.

Acknowledgement

We acknowledge various contributions by Messrs. Brian Marple, Srikant Gollapudi and Indrajit Charit, and the work described here is supported by the United States National Science Foundation grants DMR-0412583 and DMR-0968825.

References

[1] K.L.Murty, *Trans. Indian Inst. Met.,* 50 (1997) 533.
[2] K.L.Murty, *JOM,* 10 (1999) 32.
[3] E.W.Collins, *The physical metallurgy of Titanium alloys*, ASM, Metals Park, OH, 1984.
[4] K.L.Murty and B.L.Adams, *Mat. Sci. Eng.,*70(1985) 169.
[5] S.Gollapudi, I.Charit and K.L.Murty, *Acta Mater*., 56(2008) 2406.
[6] G. Srikant, B. Marple, I. Charit and K.L. Murty, *Mater. Sci. Eng.,*A463 (2007) 203.
[7] C.S. Seok, B.K. Bae, J.M. Koo and K. Linga Murty, *Eng. Failure Analysis,*13 (2006) 389.
[8] Y. Zhou, B. Devarajan and K.L. Murty, *Nuclear. Eng. Design*, 228 (2004) 3.
[9] C.S. Seok, B. Marple, Y.J. Song, S. Gollapudi, I. Charit, K.L. Murty, *Nuclear Eng. Design*, 241 (2011) 599.
[10] S. Arsene, and J. Bai, *JTEVA,*24 (1996) 386.
[11] O.A. Ruano, O.D. Sherby, *Mater. Sci. Eng.,*56A (1982) 167.
[12] S. Gollapudi, V. Bhosle, I. Charit and K. L. Murty, *Phil Mag.,*88:9 (2008) 1357.
[13] J.R. Spingarn and W.D. Nix, *Acta Metall.,*27 (1979) 171.
[14] J. Weertman, *J. Appl. Phys.,*26 (1955) 1213.
[15] J.E. Bird, A.K. Mukherjee and J.E. Dorn, in *Quantitative Relation Between Properties and Microstructure,* (ed.) D.G. Brandon and A. Rosen, Israel University Press, Jerusalem (1969) p. 255.
[16] C.R. Barrett and W.D. Nix, *Acta Met.,* 13 (1965) 1247.
[17] K. Linga Murty, M. Gold and A.L. Ruoff, *J. Appl. Phys.,*41 (1970) 4917.
[18] S. Karthikeyan, G.B. Viswanathan and M.J. Mills, *Acta Mater.,*52 (2004) 2577.
[19] J.Ravi, Wiratmo and K.L.Murty, *Nucl. Eng. Design,*156 (1995) 359.
[20] K.L.Murty, *Trans. IIM*, 53 (2000) pp. 107-120.